Unique coordination of pyrazine in $T[Ni(CN)_4] \cdot 2pyz$ with $T = Mn$, Zn, Cd

A.A. Lemus-Santana [a], J. Rodríguez-Hernández [b], L.F. del Castillo [a,*], M. Basterrechea [b], E. Reguera [b,c,**]

[a] *Departamento de Polímeros, Instituto de Investigaciones en Materiales, Universidad Nacional Autónoma de México, México*
[b] *Instituto de Ciencia y Tecnología de Materiales, Universidad de La Habana, La Ciudad de La Habana, Cuba*
[c] *Centro de Investigación en Ciencia Aplicada y Tecnología Avanzada del IPN, Unidad Legaría, México*

ARTICLE INFO

ABSTRACT

The materials under study, $T[Ni(CN)_4] \cdot 2pyz$ with $T = Mn$, Zn, Cd, were prepared by separation of $T[Ni(CN)_4]$ layers in citrate aqueous solution to allow the intercalation of the pyrazine molecules. The obtained solids were characterized from chemical analyses, X-ray diffraction, infrared, Raman, thermogravimetry, UV–Vis, magnetic and adsorption data. Their crystal structure was solved from *ab initio* using direct methods and then refined by the Rietveld method. A unique coordination for pyrazine to metal centers at neighboring layers was observed. The pyrazine molecule is found forming a bridge between Ni and T atoms, quite different from the proposed structures for $T = Fe$, Ni where it remains coordinated to two T atoms to form a vertical pillar between neighboring layers. The coordination of pyrazine to both Ni and T atoms minimizes the material free volume and leads to form a hydrophobic framework. On heating the solids remain stable up to 140 °C. No CO_2 and H_2 adsorption was observed in the small free spaces of their frameworks.

© 2009 Elsevier Inc. All rights reserved.

1. Introduction

The solids herein studied are obtained from a precursor with a layered structure, $T[Ni(CN)_4] \cdot xH_2O$, where neighboring layers remain together through van der Waals forces or hydrogen bonding interactions whether the interlayers region is occupied by water molecules. Related to these weak interactions between layers, analog solids with layered structure are usually considered as two-dimensional (2D) materials where their physical and chemical properties are dominated by that structural feature [1]. In nature many solids with layered structure are found, among them graphite, clay minerals, double hydroxides (hydrotalcite-like compounds), tetravalent metal phosphates, metal chalcogenides and polysilicates, etc. [2]. Many others synthetic analogs are also known [3]. The solids with layered structure have relatively high specific surface, from 100 to 1000 m^2/g [4]. However, the region between layers is usually accessible only for small molecules with appropriate properties to compel the layers separation, for instance, the water adsorption by clays minerals with the corresponding material swelling. To be possible the layers surface accessibility, their partial separation is required. This is achieved incorporating vertical supports or columns (pillars) between

layers. The incorporation of pillars in layered solids is a usual route to obtain porous solids with tailored cavity geometry and volume. The pillars species could also be used to incorporate certain functionality to the obtained porous solid. The pillars species selection for a given layered solid depends on the surface layers properties. For instance, in clays minerals the layers have certain charge unbalancing and in the interlayers region exchangeable cations are found. The cationic exchange with a voluminous species, like the *Keggin ion*, $[Al_{13}O_4(OH)_{24} \cdot 12H_2O]^{7+}$, leads to the increase for the interlayers distance [5].

The tetracyanonickelate ion, $[Ni(CN)_4]^{2-}$, related to its planar structure, forms layered solids when precipitates with divalent transition metals (T) which bridge neighboring planar blocks through their N ends. The separation and pillars incorporation between the formed layers, $T[Ni(CN)_4]$, has been reported for $T = Fe$ with pyridine [6] and pyrazine (pyz) [7,8], and for $T = Co$, Ni with pyrazine [8,9], 4,4′-bipyridine (bpy) and 4,4′-dipyridylacetylene (dpac) [9] as pillars. The use of pillars molecule capable of bridge formation between metal centers at neighboring layers, e.g. pyz, bpy and dpac, allows the preparation of 3D porous framework of tailored geometry. Such porous solids have been evaluated for hydrogen storage in order to shed light on the role of the pore dimension and geometry on the H_2 adsorption [8,9]. According to the structural characterization reported for the porous solids obtained, the pillar molecules are found bridging T metal centers on neighboring layers as vertical columns to form structures based on a tetragonal unit cell ($P4/m$ space group) [8,9]. The series $Fe_{1-x}T_x[M(CN)_4] \cdot pyz$ where $T = Co$, Ni and $M = Ni$, Pd,

* Corresponding author.
** Corresponding author at: Instituto de Ciencia y Tecnología de Materiales, Universidad de La Habana, Ciudad de La Habana, Cuba. Fax: +53 7 29 6000x55049.
 E-mail addresses: lfelipe@servidor.unam.mx
(L.F. del Castillo), ereguera@yahoo.com (E. Reguera).

Pt, has been intensively studied related with the spin-crossover behavior for the iron atom which shows a pronounced hysteresis loop [7,10–12]. For the remaining divalent transition metals (T = Mn, Cu, Zn, Cd), pillared compounds based on $T[Ni(CN)_4]$ has not been reported. In this contribution the preparation and characterization of $T[Ni(CN)_4] \cdot 2pyz$ frameworks with T = Mn, Zn and Cd are discussed. The study of layered cyanometalates is an active research area in solid state chemistry from decades ago [13]. The obtained solids were characterized from chemical analyses, X-ray energy-disperse spectroscopy (EDS), X-ray diffraction (XRD), infrared (IR), Raman, UV–Vis, magnetic, thermogravimetric (TG), scanning electron microscopy (SEM) and CO_2 and H_2 adsorption data.

2. Experimental section

The materials under study were prepared in two stages. Firstly, the layered structure $T[Ni(CN)_4]$ is obtained, and then the pyrazine pillars between neighboring layers are incorporated. The starting layered solids, $T[Ni(CN)_4]$, are obtained by mixing 0.1 M aqueous solutions of $K_2[Ni(CN)_4] \cdot xH_2O$ and TCl_2 (T = Mn, Cd) or $ZnSO_4$ under continuous stirring. The precipitated solid is then separated from the mother liqueur and washed several times with distilled water in order to remove all the accompanied ions. For the second stage, the formed layers are separated (detached) in a 0.3 M solution of citric acid followed by addition, drop by drop, of a diluted solution of ammonium hydroxide solution (20% v/v) until the precipitate disappearance. A solution of pyrazine (0.07 M) is then added under stirring and the formation of the pillared solid is achieved when the solution pH is adjusted to be in the 4–5 range, by adding the appropriate amount of diluted citric acid. The precipitate formed within the mother liqueur is then maintained for 12 h at 60 °C in a sealed flask before the solid fraction separation by centrifugation at room temperature. The obtained product is washed several times with distilled water and then air dried until it had constant weight. From 5 mmol of both the complex anion and the involved metal, and 0.07 mmol of pyrazine, about 100 mg of dried solid were obtained. That amount of dried solid represents a yielding of 40%, 49%, and 58% for Mn, Zn and Cd, respectively. The samples prepared according to that synthetic route were characterized from chemical analyses, EDS, XRD, IR, Raman, UV–Vis, TG, SEM and adsorption data.

EDS spectra were recorded with a Noran analytical system coupled to a SEM microscope from Jeol (Japan). This microscope was also used to obtain the SEM images. The elemental analyses were carried out with a Fisons Elemental Analyzer Model EA1108, using He as carrier/reference gas at a flow rate of 120 mL/min, and a TCD detector. The TG curves were run using a high resolution TA Instrument (Hi-ResTM) thermo-gravimetric analyzer TGA 2950 and instrument control software thermal advantage version 1.1A. The TGA 2950 was used in dynamic rate mode where the heating rate is varied dynamically according to a ramp in response to the derivative of weight change (as derivative increases, heating rate is decreased and vice versa). The heating rates were constrained to be at the 0.001 to 5 K/min range with an instrumental resolution of 5. The furnace purge was nitrogen using flow rates of 100 mL/min. IR spectra were collected by the KBr pressed disk technique using an FT spectrophotometer (Spectrum One from Perkin–Elmer). Raman spectra were collected in the 3500–100 cm^{-1} frequency range, an Almega XR dispersive Raman spectrometer equipped with an Olympus microscope (BX51) was used to obtain the Raman spectra. An Olympus ×50 objective (N.A. = 0.80) was used both for focusing the laser on the sample and collecting the scattered light in a 180° backscattering configuration. The scattered light was detected by a charge coupled device (CCD)

detector, thermoelectrically cooling to −50 °C. The spectrometer used a grating (675 lines/mm) to resolve the scattered radiation and a notch filter to block the Rayleigh light. Raman spectra were accumulated over 25 s with a resolution of $\sim 4 \, cm^{-1}$. The excitation source was 532 nm radiation from a Nd:YVO$_4$ laser (frequency-doubled) and the incident power at the sample was of ~ 2.5 mW. UV–Vis spectra were recorded with a Perkin–Elmer spectrometer using the integration sphere method.

The CO_2 and H_2 adsorption data were recorded using an ASAP 2020 analyzer (from Micromeritics). Sample tubes of known weight were loaded with an appropriate amount of sample, ~ 40 mg, and sealed using TranSeal. Previous to the CO_2 and H_2 adsorption, the samples were degassed on the ASAP analyzer at room temperature until a stable outgas rate below 1 μm Hg was obtained. The degassed sample and sample tube were weighed and then transferred back to the analyzer (with the TranSeal to prevent exposure of the sample to air). After volume measurement with He, the degassing was continued for 24 h at 60 °C in the analysis port. Measurements were performed at 75 K in liquid N_2 for H_2 and at 273 K within an ice-water bath for CO_2.

The XRD powder patterns were recorded in the Bragg–Brentano geometry using Cu$K\alpha$ radiation and a D8 Advance (from

Table 1
Crystallographic data for the refined structures.

Data collection		
Diffractometer	D8 Advance (from Bruker)	
Monochromator	Graphite	
Wavelength (Å)	Cu$K\alpha$ = 1.54183	
2θ range (deg)	5–90	
Step size (deg)	0.025	
Time per step (s)	15	

	Zn[Ni(CN)$_4$]·2pyz	Mn[Ni(CN)$_4$]·2pyz
Unit cell		
Space group	Pnc2	Pnc2
Parameter (Å)	a = 6.8199(2)	a = 6.7808(2)
	b = 13.9699(3)	b = 13.9571(4)
	c = 7.2927(2)	c = 7.2607(2)
V (Å^3)	694.8(1)	687.1(2)
Z	2	2
Refinement		
Number of contributing reflections	318	312
Number of distance constraints	4	4
Number of refined parameters		
Structural parameters	41	41
Profile parameters	10	10
R_{exp}	2.50	3.28
R_{wp}	5.82	7.21
R_B	4.59	7.35
S	2.32	2.19

	Cd[Ni(CN)$_4$]·2pyz
Unit cell	
Space group	Pnc2
Parameter (Å)	a = 6.9776(2)
	b = 14.1719(3)
	c = 7.4717(2)
V(Å^3)	738.8(4)
Z	2
Refinement	
Number of contributing reflections	334
Number of distance constraints	4
Number of refined parameters	
Structural parameters	41
Profile parameters	10
R_{exp}	3.41
R_{wp}	9.7
R_B	8.9
S	2.8

Bruker). Some XRD powder patterns were collected at the XPD-10B beamline at the LNLS synchrotron radiation facility (Campinas, Brazil), under vacuum (10^{-6} mmHg) at room temperature and at 50, 120 and 170 °C. The wavelength used was 1.549830 Å (7.9998 keV). All the patterns were collected from 5° to 100°/2θ with a step size of 0.025°. The experimental details are summarized in Table 1. The crystal structures were solved *ab initio*
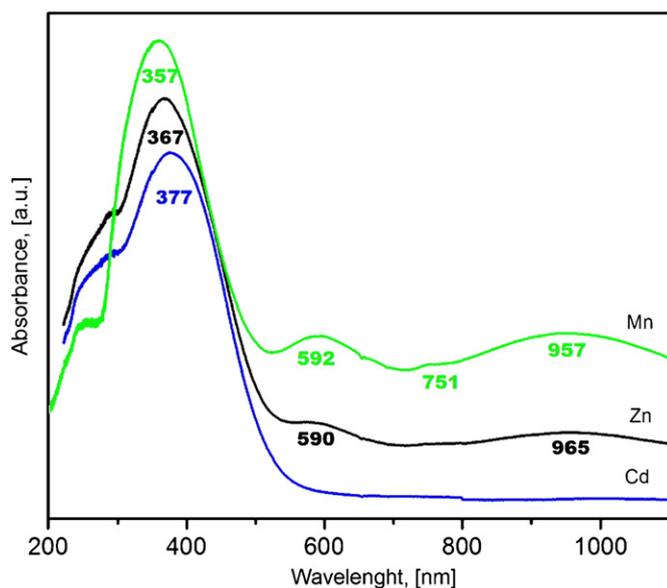
by direct methods using the program SHELXS [14] from extracted intensities according to the Le Bail method [15]. Physical considerations and information from the remaining techniques were used in order to select the appropriate structural models to be refined, and then to check the obtained structure. The structural refinement from these XRD powder patterns was performed with the Rietveld method using the FullProf program [16] and pseudo-Voigt peak shape function. Peak profiles were calculated within 10 times the full width at half maximum (FWHM). The background was modeled by a third-order polynomial. The interatomic C–N and Ni–C distances were constrained to take values within certain limits considering results from single crystal studies of cyanometallates [17]. The materials framework 3D illustration and the available free spaces and slit size were calculated from the refined crystal structure.

3. Results and discussion

3.1. Nature of the solids under study

The obtained powders have characteristic colors: yellow–greenish for Mn and Zn, and yellow for Cd. These colors indicate the occurrence of a pronounced light absorption in the blue spectral region, probably related to photo-induced metal-to-ligands charge transfer processes. This was confirmed from the recorded UV–Vis spectra (Fig. 1). Transition metal cyanide complexes show intense metal-to-ligands charge transfer absorption bands in that region [18]. From EDS analyses atomic metal ratios close to 1:1 were obtained, corresponding to the expected formula unit $T[Ni(CN)_4]$ for the layered structures. IR spectra (discussed below) revealed that pyrazine was incorporated into the formed solids as a bridge ligand between metal centers. The coordination of pyrazine to a metal center leads to detectable
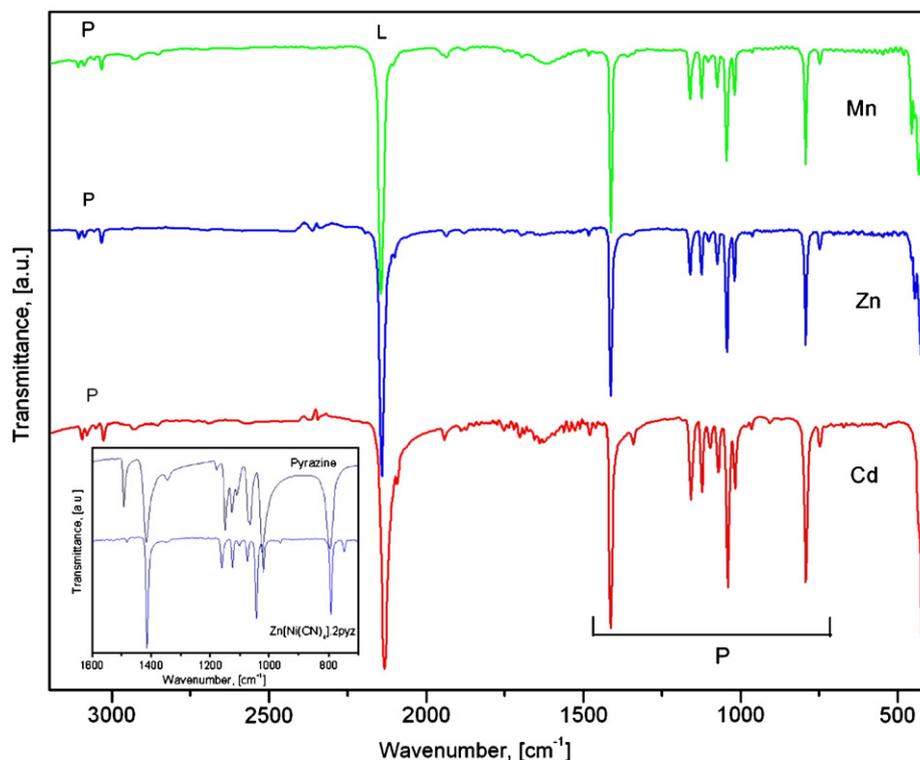

Fig. 1. UV–Vis spectra for the series $T[Ni(CN)_4] \cdot 2pyz$ with $T = $ Mn, Zn, Cd. For Mn and Zn weak bands above 500 nm characteristic of the Ni(II) atom, d^8 ion, in a slightly distorted octahedral environment are observed. The strong bands below observed 500 nm were ascribed to metal-ligand charge transfers.

Fig. 2. IR spectra for $T[Ni(CN)_4] \cdot 2pyz$ with $T = $ Mn, Zn, Cd. These spectra can be considered as formed by the contributions from the layered structure ($T[Ni(CN)_4]$), and the pyrazine molecules (P). The intense band in the 2200–2100 spectral region (L) corresponds to the ν(CN) vibration. Inset: IR spectra for pyrazine and $Zn[Ni(CN)_4] \cdot 2pyz$. On the pyrazine coordination to the metal centers pronounced changes are observed for pyrazine ring vibrations accompanied of frequency shift for their absorption bands.

Table 2
Frequencies in (cm^{-1}) for the IR absorption bands corresponding to the layers of the studied series $T[Ni(CN)_4] \cdot 2pyz$ with $T = Mn, Zn, Cd$.

Compound	$[Ni(CN)_4]$			pyz^a					
	$v(CN)$	$v(NiC)$	$\delta(NiCN)$	$v(CH)$	v_{ring}	γ_{ring}	δ_{ring}	$\delta(CH)$	$\gamma(CH)$
$K_2[Ni(CN)_4] \cdot H_2O$	2123	457[b]	418						
$Mn[Ni(CN)_4] \cdot xH_2O$	2156	479	439						
$Zn[Ni(CN)_4] \cdot xH_2O$	2193	572	459						
$Cd[Ni(CN)_4] \cdot xH_2O$	2140	549	433						
pyz	–	–	–	3083 3061 3011 2971	1492 1417	1150	1024	1125 1065	795
$Mn[Ni(CN)_4] \cdot 2pyz$	2144	546[c]	434	3109 3090 3059 3034	1483 1414	1162 1020 749 458[b] 447[b]	1046	1125 1075	794
$Zn[Ni(CN)_4] \cdot 2pyz$	2142	543[c]	424	3107 3088 3058 3034	1414	1161 1020 749 457[b] 447[b]	1044	1125 1075	793
$Cd[Ni(CN)_4] \cdot 2pyz$	2132	540[c]	420	3097 3080 3050 3027	1415	1160 1020 749 435	1041	1124 1073	792

[a] Ref. [19].
[b] Shoulder.
[c] Very weak band.
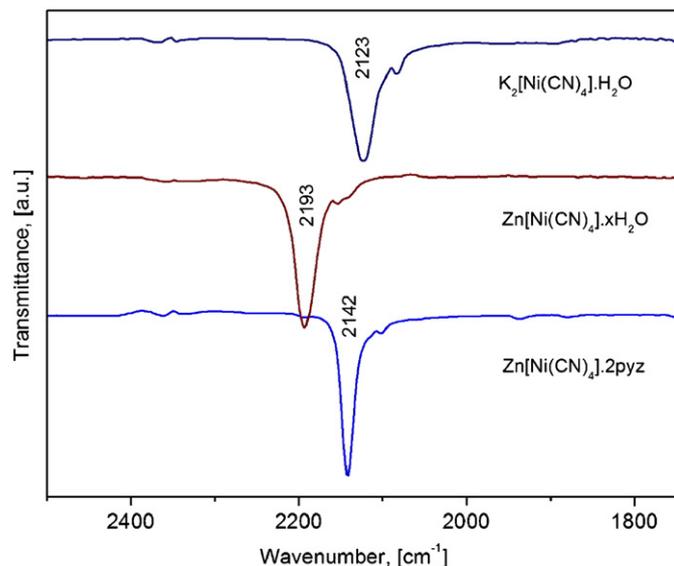
Fig. 3. Frequency shift for the $v(CN)$ stretching band on the Zn atom coordination to the N ends of the CN groups and then when the pyrazine molecule coordinates the metal centers on neighboring layers.
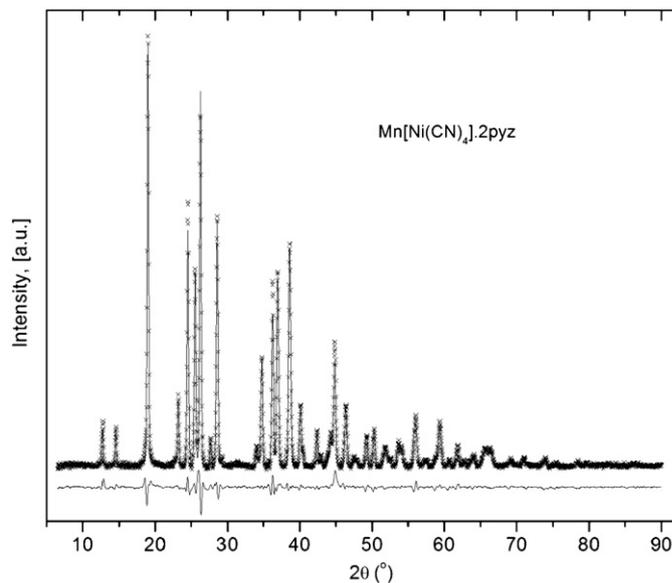
Fig. 4. XRD powder patterns, experimental and fitted, and their difference for $Mn[Ni(CN)_4] \cdot 2pyz$.

frequency shifts for some absorption bands of its IR spectrum [19]. The chemical analyses, which are summarized as follow, in %: Mn (Calc.: C, 38.14; N, 29.63; H, 2.13; Exp.: C, 37.7; N, 29.03; H, 1.81); Zn (Calc.: C, 37.11; N, 28.85; H, 2.07; Exp.: C, 36.36; N, 27.08; H, 1.73); Cd (Calc.: C, 33.10; N, 25.73; H, 1.85; Exp.: C, 32.84; N, 24.38;

H, 1.50) indicated that two pyrazine molecules per formula unit of metal tetracyanonickelate are present in the solids. This is consistent with the TG data where the weight lost on heating, before the metal cyanide decomposition, corresponds to the evolution of two pyrazine molecules per formula unit (discussed
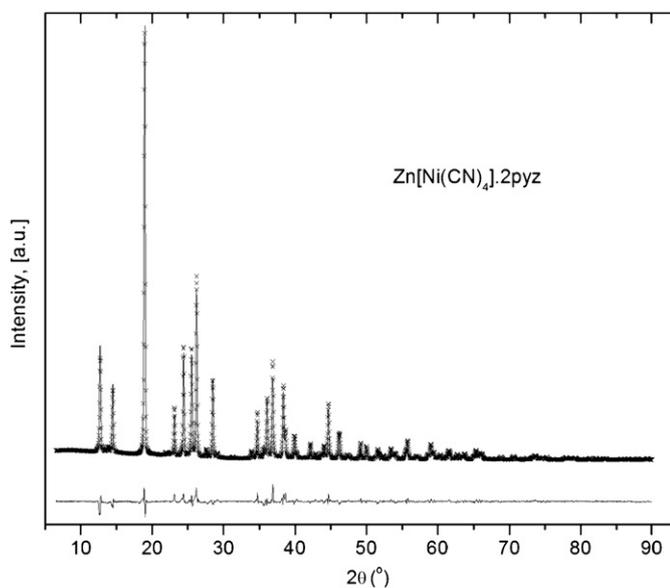
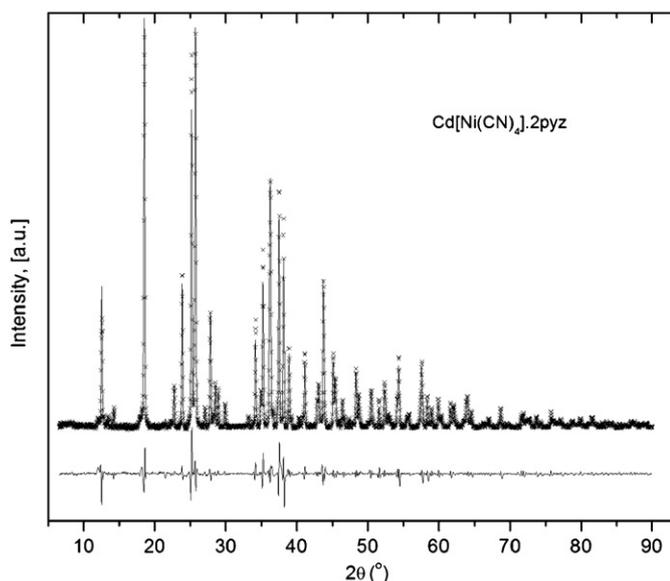**Fig. 5.** XRD powder patterns, experimental and fitted, and their difference for $Zn[Ni(CN)_4] \cdot 2pyz$.

Fig. 6. XRD powder patterns, experimental and fitted, and their difference for $Cd[Ni(CN)_4] \cdot 2pyz$.

Table 3
Atomic positions and temperature (Biso) and occupation (Occ) factors for the refined crystal structures.

Composition	Site	x	y	z	Biso	Occ
$Zn[Ni(CN)_4] \cdot 2pyz$						
Zn	2a	0	0	0.391(3)	1.94(2)	1
Ni	2b	0.5	0	0.887(2)	2.05(2)	1
C1	4c	0.659(6)	0.036(2)	0.702(4)	2.5(1)	1
N1	4c	0.781(4)	0.055(1)	0.593(3)	2.5(1)	1
C2	4c	0.314(5)	−0.026(2)	1.059(4)	2.5(1)	1
N2	4c	0.206(3)	−0.036(1)	1.173(3)	2.5(1)	1
N3	4c	0.147(2)	0.154(1)	0.375(6)	3.1(2)	1
C3	4c	0.017(3)	0.227(1)	0.413(6)	3.1(2)	1
C4	4c	0.355(2)	0.157(1)	0.390(8)	3.1(2)	1
C5	4c	0.121(2)	0.310(1)	0.381(8)	3.1(2)	1
C6	4c	0.427(3)	0.251(1)	0.423(4)	3.1(2)	1
N4	4c	0.314(2)	0.320(1)	0.413(5)	3.1(2)	1
O1	4c	0.578(3)	0.228(1)	0.259(4)	6.2(3)	0.489(1)
$Mn[Ni(CN)_4] \cdot 2pyz$						
Mn	2a	0	0	0.389(3)	1.65(3)	1
Ni	2b	0.5	0	0.887(4)	1.82(2)	1
C1	4c	0.666(4)	0.040(7)	0.702(2)	2.7(1)	1
N1	4c	0.794(5)	0.057(4)	0.602(2)	2.7(1)	1
C2	4c	0.318(3)	−0.027(4)	1.069(3)	2.7(1)	1
N2	4c	0.192(3)	−0.034(2)	1.175(4)	2.7(1)	1
N3	4c	0.152(3)	0.150(2)	0.380(6)	3.4(2)	1
C3	4c	0.020(4)	0.236(6)	0.412(3)	3.4(2)	1
C4	4c	0.354(4)	0.156(2)	0.394(5)	3.4(2)	1
C5	4c	0.117(6)	0.312(4)	0.385(2)	3.4(2)	1
C6	4c	0.420(4)	0.246(7)	0.429(3)	3.4(2)	1
N4	4c	0.317(4)	0.321(2)	0.415(2)	3.4(2)	1
$Cd[Ni(CN)_4] \cdot 2pyz$						
Cd	2a	0	0	0.399(2)	1.54(1)	1
Ni	2b	0.5	0	0.886(3)	1.96(2)	1
C1	4c	0.658(2)	0.035(3)	0.696(2)	2.5(2)	1
N1	4c	0.772(6)	0.054(3)	0.592(4)	2.5(2)	1
C2	4c	0.316(3)	−0.029(3)	1.060(2)	2.5(2)	1
N2	4c	0.203(4)	−0.040(4)	1.170(3)	2.5(2)	1
N3	4c	0.142(3)	0.158(2)	0.376(4)	3.0(1)	1
C3	4c	0.016(4)	0.225(6)	0.409(4)	3.0(1)	1
C4	4c	0.362(2)	0.157(1)	0.405(4)	3.0(1)	1
C5	4c	0.119(3)	0.309(4)	0.387(3)	3.0(1)	1
C6	4c	0.430(4)	0.252(2)	0.430(4)	3.0(1)	1
N4	4c	0.322(2)	0.312(3)	0.423(3)	3.0(1)	1

below). According to both TG and IR data, all the samples were found to be anhydrous solids, and the overall formula unit results $T[Ni(CN)_4] \cdot 2pyz$. The morphology of the formed powders, as detected from SEM images (see Supplementary information), is typical of crystalline materials formed by single particles of well defined faces and edges, which was corroborated from XRD patterns (discussed below).

3.2. IR and Raman spectra

Fig. 2 shows the IR spectra for the series $T[Ni(CN)_4] \cdot 2pyz$. These spectra can be considered as the contributions from the two involved building units, the layered structure, $T[Ni(CN)_4]$, and the pyrazine molecule as bridge ligand. The incorporation of pyrazine into the solids is detected by the presence of a set of sharp absorption bands in the 3100–3000 cm^{-1} spectral region, ascribed to $v(CH)$ vibrations, clearly shifted to upward frequencies in comparison with the free pyrazine. The coordination bond formation involves the charge donation to the metal centers, which is partially removed from the pyrazine ring. This is the reason for $v(C–H)$ vibrations incremental frequency observed as weak absorption bands above 3000 cm^{-1} (Fig. 2). Vibrations involving the pyrazine ring display a pattern of bands below 1500 cm^{-1} (Fig. 2) in which practically all bands undergo noticeable shifts and large changes in the absorption bands intensity (Fig. 2, Inset). The same behavior was observed from the recorded Raman spectra (see Supplementary information).

Among pyrazine ring vibrational pattern, δ and γ modes are the most affected (Table 2), in total agreement with a classic harmonic oscillator model of IR vibrations, which explains the observed frequency shift as an increase on the strain as a consequence of (pyz) N–T bond formation. Worthy of note are a couple of bands (457 and 447 cm^{-1}) displayed as shoulders in the low frequency region of the spectra when T = Mn and Zn. Their presence at these specific frequencies points out the possibility of an asymmetric N_{ring} coordination to the metal, i.e., although bridging, one of the

Table 4

Distances (Å) and bond angles (deg) for the refined structures.

	Bond distance (Å)	Angles (deg)	
$Zn[Ni(CN)_4] \cdot 2pyz$			
	Ni–C1 = 1.811(2)	C1–Ni–C2 = 172.3(2)	N2–Zn–N3′ = 91.5(2)
	Ni–C2 = 1.822(4)	C1–Ni–C1′ = 83.2(8)	Zn–N1–C1 = 146.9(6)
	Zn–N1 = 2.239(1)	C1–Ni–C2′ = 92.6(6)	Zn–N2–C2 = 159.5(1)
	Zn–N2 = 2.182(4)	C2–Ni–C2′ = 92.8(1)	Zn–N3–C3 = 112.8(1)
	Zn–N3 = 2.379(1)	Ni–C1–N1 = 171.9(8)	Zn–N3–C4 = 116.4(8)
	C1–N1 = 1.172(1)	Ni–C2–N2 = 173.9(3)	N3–C3–C5 = 104.9(1)
	C2–N2 = 1.115(3)	N1–Zn–N1′ = 97.3(8)	C3–C5–N4 = 124.0(4)
	N3–C3 = 1.381(4)	N1–Zn–N2 = 172.4(7)	C5–N4–C6 = 122.4(6)
	C3–C5 = 1.383(7)	N1–Zn–N2′ = 88.1(5)	N4–C6–C4 = 119.9(8)
	C5–N4 = 1.345(3)	N1–Zn–N3 = 90.1(1)	C6–C4–N3 = 112.5(1)
	N4–C6 = 1.238(6)	N1–Zn–N3′ = 93.5(5)	C4–N3–C3 = 126.9(8)
	C6–C4 = 1.419(1)	N2–Zn–N2′ = 86.8(1)	
	C4–N3 = 1.427(4)	N2–Zn–N3 = 84.4(4)	
$Mn[Ni(CN)_4] \cdot 2pyz$			
	Ni–C1 = 1.839(2)	C1–Ni–C2 = 173.3(9)	N2–Mn–N3′ = 92.9(1)
	Ni–C2 = 1.846(3)	C1–Ni–C1′ = 86.2(6)	Mn–N1–C1 = 146.3(3)
	Mn–N1 = 2.230(6)	C1–Ni–C2′ = 92.9(6)	Mn–N2–C2 = 160.3(1)
	Mn–N2 = 2.081(3)	C2–Ni–C2′ = 88.6(3)	Mn–N3–C3 = 116.4(3)
	Mn–N3 = 2.334(4)	Ni–C1–N1 = 168.6(2)	Mn–N3–C4 = 119.4(2)
	C1–N1 = 1.156(2)	Ni–C2–N2 = 171.5(3)	N3–C3–C5 = 109.5(1)
	C2–N2 = 1.154(1)	N1–Mn–N1′ = 92.2(1)	C3–C5–N4 = 124.3(2)
	N3–C3 = 1.515(2)	N1–Mn–N2 = 172.0(2)	C5–N4–C6 = 118.7(3)
	C3–C5 = 1.263(4)	N1–Mn–N2′ = 92.5(2)	N4–C6–C4 = 124.7(3)
	C5–N4 = 1.379(3)	N1–Mn–N3 = 88.6(2)	C6–C4–N3 = 113.5(2)
	N4–C6 = 1.262(5)	N1–Mn–N3′ = 93.6(2)	C4–N3–C3 = 121.9(1)
	C6–C4 = 1.357(5)	N2–Mn–N2′ = 83.4(4)	
	C4–N3 = 1.376(1)	N2–Mn–N3 = 84.7(1)	
$Cd[Ni(CN)_4] \cdot 2pyz$			
	Ni–C1 = 1.864(2)	C1–Ni–C2 = 172.8(4)	N2–Cd–N3′ = 88.3(2)
	Ni–C2 = 1.872(2)	C1–Ni–C1′ = 80.8(3)	Cd–N1–C1 = 146.7(1)
	Cd–N1 = 2.279(4)	C1–Ni–C2′ = 93.7(2)	Cd–N2–C2 = 157.5(1)
	Cd–N2 = 2.292(4)	C2–Ni–C2′ = 92.1(3)	Cd–N3–C3 = 112.0(2)
	Cd–N3 = 2.454(3)	Ni–C1–N1 = 172.2(1)	Cd–N3–C4 = 112.4(3)
	C1–N1 = 1.144(2)	Ni–C2–N2 = 175.1(1)	N3–C3–C5 = 104.3(2)
	C2–N2 = 1.149(2)	N1–Cd–N1′ = 101.5(1)	C3–C5–N4 = 120.4(2)
	N3–C3 = 1.317(3)	N1–Cd–N2 = 170.5(4)	C5–N4–C6 = 129.5(2)
	C3–C5 = 1.400(2)	N1–Cd–N2′ = 87.5(3)	N4–C6–C4 = 118.3(3)
	C5–N4 = 1.442(3)	N1–Cd–N3 = 91.1(3)	C6–C4–N3 = 109.6(2)
	N4–C6 = 1.137(4)	N1–Cd–N3′ = 93.9(4)	C4–N3–C3 = 129.8(2)
	C6–C4 = 1.439(6)	N2–Cd–N2′ = 83.4(4)	
	C4–N3 = 1.550(3)	N2–Cd–N3 = 85.6(3)	

coordination interaction is a very weak one [20]. On the other hand, in the case of Cd there is just a weak shoulder at 435 cm⁻¹, and there are no bands in this region which can support a bridging mode [19].

Regarding the layered structure contribution to the IR spectra of the pillared compositions, it is convenient to follow the changes in the spectrum on the *T* metal coordination to the N ends of the starting $[Ni(CN)_4]^{2-}$ building block during the layers preparation, and then on the pyrazine pillars incorporation between the layers. The formation of the layered structure from the solutions of $[Ni(CN)_4]^{2-}$ and T^{2+} is detected as an upward shift for the $v(CN)$ vibration, which amounts 33 (Mn), 70 (Zn) and 17 (Cd) cm⁻¹ (Fig. 3, Table 2). The binding of the metal (*T*) to the N end involves charge donation from the 5σ orbital of the CN group which has certain anti-bonding character. From this fact, the ligand-to-metal charge donation is detected as a frequency increase for the IR allowed E_u $v(CN)$ vibration. The observed frequency shift depends on the ability of the involved *T* metal to subtract charge from the CN group. For Zn the highest $v(CN)$ frequency shift (70 cm⁻¹) was observed (Fig. 3). The 4s orbital of the Zn atom has a relatively low energy to be able the charge redistribution within the atom, receiving charge from its 3d orbitals, to allow the ligand-to-metal

charge donation in the resulting partially unoccupied metal 3d orbitals. The charge redistribution within the Zn atom results from an induced effect by the metal-ligand interaction. These 3d orbitals have a high ability to receive electron density from the 5σ orbital of the CN group to favor a $3d^{10}$ electronic configuration in the Zn atom. This could explain the large frequency shift, of 70 cm⁻¹, observed when the layered structure is formed from Zn atoms. For Cd, which has a larger ionic radius and a lesser polarizing power, the frequency shift is significantly less pronounced, of only 17 cm⁻¹. The low frequency IR allowed vibrations $v(NiC)$ (E_u) and $\delta(NiCN)$ (E_u) are also sensitive to the salt formation with the metal at the N end but with a smaller frequency shift (Table 2). The charge removal from the ligand at the N end induces a greater π-back donation at the C end and this strengthens the Ni–C bond and an increase for the $v(NiC)$ frequency is detected. This is a well-known induced effect in hexacyanometallates [21,22]. From Raman spectra the same behavior is observed (see Supplementary information).

The water-replacing ligands to the *T* metal have an inverse effect. The charge donated by the N donor ligand (pyrazine) in comparison with O donor ligand (water) reduces the metal ability to subtract charge from the CN group and this is detected as a

decrease for the v(CN) frequency in both IR and Raman spectra. The same evidence is obtained when IR spectra of anhydrous and hydrated layered solids are compared with the one to pyrazine containing composition (see Supplementary information). In the studied series $T[\text{Ni(CN)}_4]\cdot 2\text{pyz}$ that frequency decrease is 7 (Mn), 51 (Zn), 8 (Cd) cm^{-1} (see Fig. 3 and Table 2). The pyrazine coordination to the metal centers leads to a pronounced charge redistribution in the T–N–C–Ni chain, particularly pronounced for Zn. The same behavior was observed from the Raman data. The pyrazine molecule interaction with the Ni atom takes place through the metal partially occupied $3d_z^2$ orbital, with probably a minor effect on the frequency for the v(CN) stretching vibration. This vibration mainly involves metal orbitals located on the layer plane.

3.3. Crystal structures

The materials under study are obtained as polycrystalline powders. From the recorded XRD powder patterns the unit cell of these powders were found to be orthorhombic. That unit cell agrees with the observed morphologies for the formed micro-crystals. The recorded SEM images correspond to materials with an orthorhombic structure (see Supplementary information). A crystal model in the space group $Pnc2$, consistent with the above discussed spectroscopic information was derived from the extracted intensities using the Le Bail method [14]. Physical considerations were also used to restraint the variation limits for the Ni–C and C–N interatomic distances and C–Ni–C and Ni–C–N bond angles. Due to the nature of the bonding structure, for the Ni–C–N chain no large deviations from the linearity are expected. Figs. 4–6 show the experimental and fitted XRD powder patterns and their differences for the studied series of compounds. The obtained values for the figures of merits corresponding to these fitting are reported in Table 1. These values are not too low as those usually obtained from single crystals XRD structure refinements but are acceptable for structural studies from XRD powder patterns. In Table 3 the refined atomic positions and thermal and occupation factors are summarized. The calculated bond distances and angles are given in Table 4.

Fig. 7 shows the atomic packing within the unit cell for this series of materials. Both Ni and T metals are found with a pseudo-octahedral coordination, NiC$_4$(N$_2$)$_{\text{pyz}}$ and T(N$_4$)$_{\text{CN}}$(N$_2$)$_{\text{pyz}}$, respectively. All the pyrazine molecules are forming bridges between Ni and T metals in the interlayers region, Ni–pyrazine–T. Along the c axis, the pyrazine molecules are found stacked according to a crossed configuration. In the 3D structure of $T[\text{Ni(CN)}_4]\cdot 2\text{pyz}$, the layers of $T[\text{Ni(CN)}_4]$ appear are rippled sheets related to a deviation for the N–T–N chains from the linearity, $\angle$ N–T–N = 174.5°, quite different from the structural feature of a layered structure, like $T[\text{Ni(CN)}_4]$. Carbon and N atoms in the CN groups are involved in a triple bond, and also Ni and the CN ligand due to the π-back bonding interaction with participation of two t_{2g} orbitals from the Ni atoms. In consequence, the Ni–C–N chain shows a relatively high rigidity. A higher flexibility and deviation from the linearity for the N–T–N angle are possible due to the nature of the involved T–N interaction, a single σ bond. To that deviation also a different bonding interaction of the pyrazine molecule with T and Ni atoms could be contributing.

The observed crystal structure found for the series $T[\text{Ni(CN)}_4]\cdot 2\text{pyz}$ is quite different from that proposed for $T[\text{Ni(CN)}_4]\cdot \text{pyz}$ with T = Fe, Co, Ni [7–12] where the pyrazine molecule only coordinates T metal centers on neighboring layers while the Ni atoms remain free of interaction with the pyrazine molecule. The crystal structure of this last series is based on a tetragonal unit cell, where the linearity for the T–N–C–Ni chains is

preserved. This suggests that the above mentioned rippled sheets structure for the studied series of orthorhombic solids is related to a different bonding interaction for the pyrazine molecule with both T and Ni atoms.

Conclusive evidence on the octahedral coordination for the Ni atom, at least for Mn and Zn is obtained from the UV–Vis spectra. Fig. 1 shows the diffuse reflectance spectra for the series of
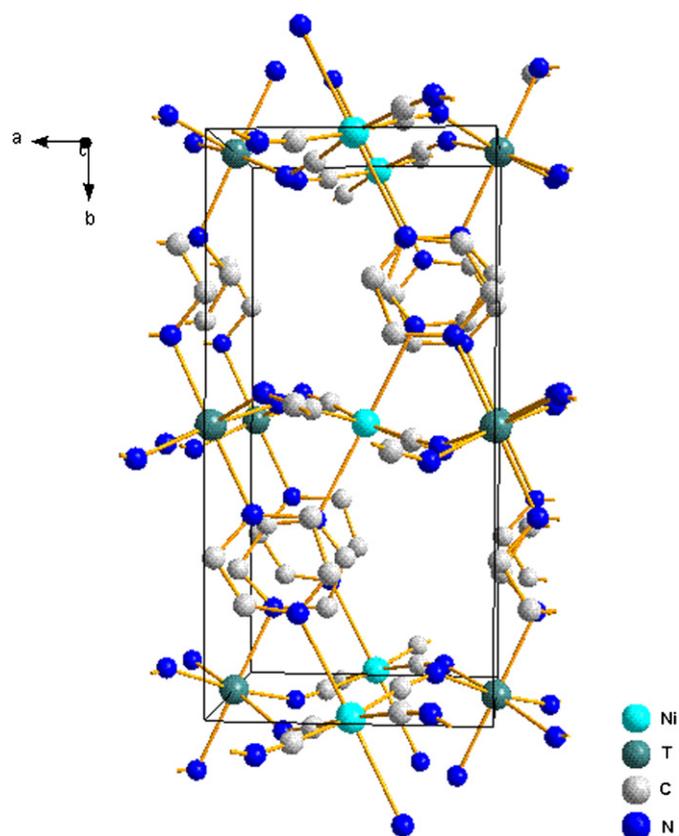

Fig. 7. Atomic packing within the orthorhombic unit cell for the series $T[\text{Ni(CN)}_4]\cdot 2\text{pyz}$ with T = Mn, Zn, Cd.

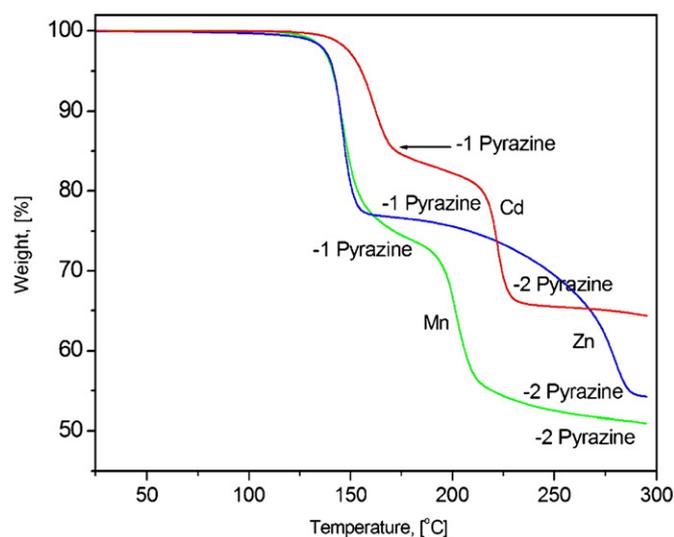**Fig. 8.** TG curves for the series $T[\text{Ni(CN)}_4]\cdot 2\text{pyz}$. From about 130 °C a first pyrazine molecule evolves to form a mono-pyrazine complex salt. The evolution of the second pyrazine molecule is detected for a heating of 160 °C for Mn and at higher temperatures for Zn and Cd.
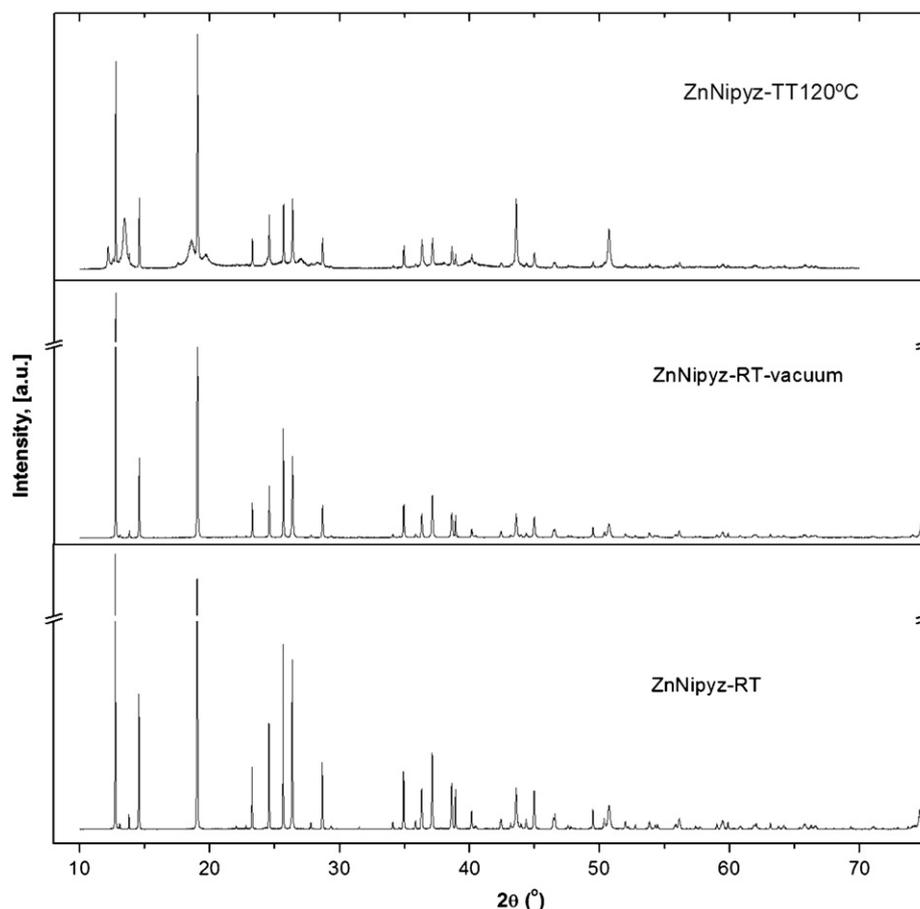
Fig. 9. XRD powder patterns for $Zn[Ni(CN)_4]\cdot 2pyz$ recorded at room temperature for the initial sample in air, under vacuum, and after a heating of 120 °C also under vacuum. On the sample heating at 120 °C a pyrazine molecule evolves and a new structure appears. The pattern recorded for a heating of 170 °C (not shown) corresponds to a material amorphous to XRD.

studied solids. For Mn and Zn bands characteristic of $3d^8$ Ni (II) ion in a slightly distorted octahedral geometry are observed. For Cd such d–d transitions do not appear or are very weak. The intense bands observed in the ultraviolet-blue region were ascribed to metal-to-ligand charge transfer (CT) transitions, usually observed in transition metal cyanides [18]. For $T =$ Zn, only two of the three expected d–d transitions are detected, at 965 and 590 nm, assigned to $^3T_{2g} \leftarrow {}^3A_{2g}(F)$, $^3T_{1g}(F) \leftarrow {}^3A_{2g}(F)$. The third transition probably is obscured by the CT band. When $T =$ Mn, besides the already mentioned bands, there is a weak transition at 751 nm assigned to $^1E_g(P) \leftarrow {}^3A_{2g}(F)$ spin–orbit coupled transition.

The results obtained from the UV–Vis spectra are corroborated by the values for the room temperature magnetic moment in the studied series of solids, $T[Ni(CN_4)]\cdot 2pyz$. For $T =$ Mn and Zn net magnetic moment of 8.1 and 2.71 μB, respectively, were obtained, while to Cd practically a diamagnetic behavior results. This atypical feature for Cd could be attributed to a particularly weak interaction of the pyrazine molecule with the Ni atom for the Cd containing solid. According to the involved frequency shift in the IR spectra on the pyrazine molecule incorporation between neighboring layers, to Cd the weakest metal-ligand interaction corresponds (see Table 2).

3.4. Thermal stability

Fig. 8 shows the TG curves for the studied series of orthorhombic solids, $T[Ni(CN)_4]\cdot 2pyz$. The absence of weight lost

Table 5
Cell parameters (Å) calculated from XRD patterns recorded at room temperature under vacuum before and after a heating of 120 °C.

Compounds	Room temperature (RT)	RT—under vacuum	RT—vacuum after a heating of 120 °C
$Mn[Ni(CN)_4]\cdot 2pyz$	$a = 6.782$ $b = 13.952$ $c = 7.259$	$a = 6.780$ $b = 13.950$ $c = 7.258$	$a = 6.777$ $b = 13.950$ $c = 7.256$
$Zn[Ni(CN)_4]\cdot 2pyz$	$a = 6.813$ $b = 13.958$ $c = 7.286$	$a = 6.815$ $b = 13.957$ $c = 7.284$	$a = 6.811$ $b = 13.951$ $c = 7.283$
$Cd[Ni(CN)_4]\cdot 2pyz$	$a = 6.981$ $b = 14.178$ $c = 7.476$	$a = 6.980$ $b = 14.176$ $c = 7.475$	$a = 6.980$ $b = 14.177$ $c = 7.473$

below 100 °C confirms their anhydrous nature. The materials framework has no available coordination sites to allow a high stabilization of water molecules in their structure, and weakly bonded water molecules usually evolve for heating temperatures below 100 °C. From about 130 °C a pronounced weight lost is detected which ends above 140 °C for Mn and Zn, and close to 160 °C for Cd. That weight lost corresponds to the evolution of a pyrazine molecule per formula unit. The evolution of the second
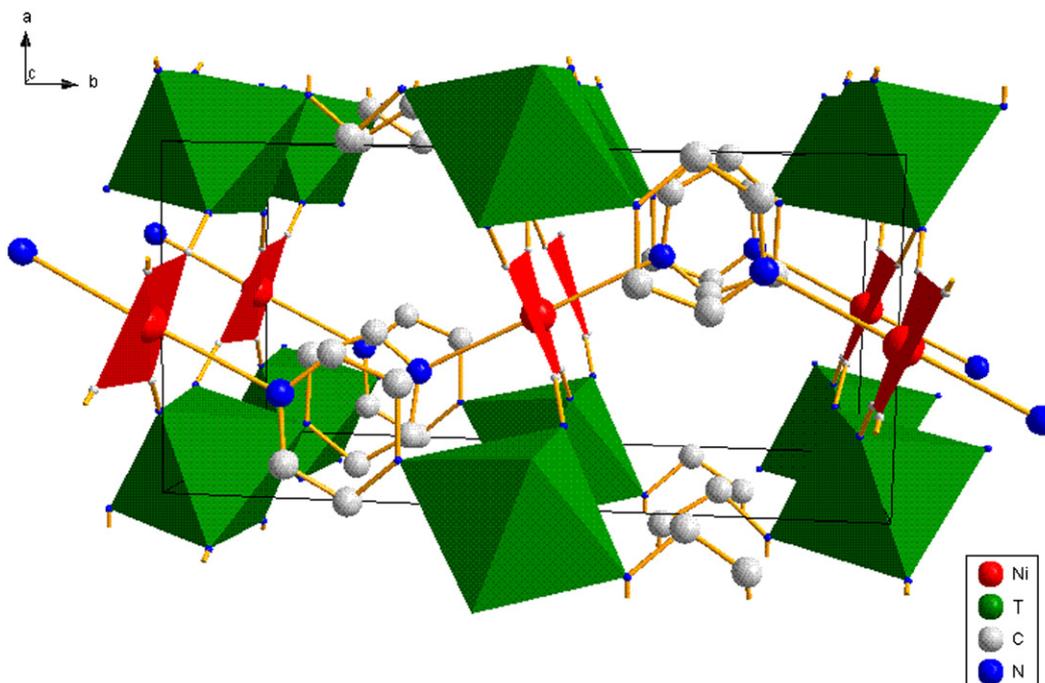
Fig. 10. Porous framework for the series $T[Ni(CN)_4] \cdot 2pyz$ with T = Mn, Zn, Cd. The available free volume is formed by relatively small cavities.

pyrazine molecule begins from about 190 °C for Mn and Zn and at slightly higher temperature for Cd.

XRD powder patterns recorded at room temperature under a vacuum of 10^{-6} mmHg for samples without previous heating and after heat treatments in vacuum at 120 °C are shown in Fig. 9 for T = Zn. The analog patterns for Mn and Cd are available from Supplementary information. In Table 5 the cell parameters calculated from these XRD patterns are summarized. The sample evacuation or its heating up to a moderate temperature, 50 °C, for instance, has no effect on the material framework. For samples heated at 120 °C a new phase appears, ascribed to the evolution of a pyrazine molecule to form the mono-pyrazine complex salt $T[Ni(CN)_4] \cdot pyz$.

3.5. Framework, adsorption data and free volume accessibility

As already mentioned, the series $T[Ni(CN)_4] \cdot pyz$ with T = Fe, Co, Ni has been evaluated for the hydrogen storage [8,9]. The porous framework of these pillared compounds result accessible for N_2 and H_2. The distance between neighboring pyrazine pillars is close to 9 Å, sufficient to accommodate the N_2 and H_2 molecules with 2.9 and 2.4 Å of van der Waals diameters, respectively [8]. According to the refined crystal structures, the series $T[Ni(CN)_4] \cdot 2pyz$ has a relatively compact framework (see Fig. 10). Three factors contribute to reduce the pore size for this framework: (a) the presence of pyrazine molecules as bridge group linking all the available metal centers on neighboring layers; (b) their sloped and crossed configuration which reduces the layer to layer distance; and (c) the rippled sheets form resulting for these layers. This last feature is also responsible for the formation of pores of irregular shape. The maximum slit width for the formed pores remains below 4 Å, for the region between neighboring pyrazine molecules, which, from preliminary adsorption studies, was found to be insufficient to allow the pore accessibility for the nitrogen molecule. From this fact, the pore accessibility study was also carried out for CO_2 and H_2. Carbon dioxide, along the O–C–O axis, has a relatively small effective cross section, sufficient to
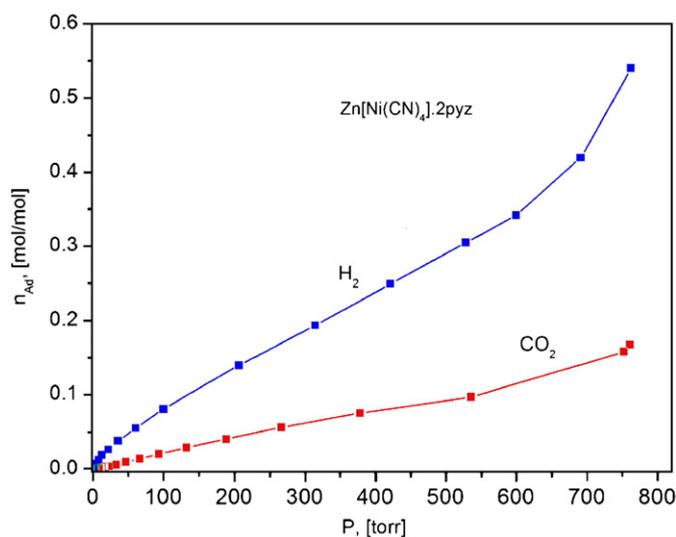

Fig. 11. H_2 and CO_2 adsorption curves for $Zn[Ni(CN)_4] \cdot 2pyz$. The porous framework of this material results inaccessible to CO_2, and practically also to H_2. These adsorption curves were recorded at 75 and 273 K for H_2 and CO_2, respectively, and with a large equilibrium time (60 s) but due to a low diffusion rate for the adsorbate in the material framework, evidence of kinetic effects are appreciated. An analogue behavior was observed for $Mn[Ni(CN)_4] \cdot 2pyz$ and $Cd[Ni(CN)_4] \cdot 2pyz$.

allow its adsorption in narrow cavities [23]. Fig. 11 shows the recorded H_2 and CO_2 adsorption curves for Zn as representative of the studied series of orthorhombic solids, $T[Ni(CN)_4] \cdot 2pyz$. The free space available in the materials framework appears to be practically inaccessible to these two probe molecules. For H_2 the adsorption curve shows an increasing slope indicating the presence of pronounced kinetic effects, even for large equilibrium times, related to a very low H_2 diffusion rate through the narrow channels system. These H_2 and CO_2 adsorption data support the refined crystal structures for the materials under study. The non-availability of free metal coordination sites on the layers and the

relatively large electron charge density on the cavities surface formed by the CN and pyrazine bridges are probably responsible for the anhydrous nature of this series of compounds. That negative charge density generates certain repulsive interaction for the water molecule within the cavity. The water molecule has a kinetic diameter of about 2.65 Å, enough small to be possible its accommodation within the cavities of these materials.

4. Conclusions

Samples for the series $T[Ni(CN)_4] \cdot 2pyz$ with $T =$ Mn, Zn, Cd were prepared and characterized. According to the refined crystal structures, the pyrazine molecule was found to be with a unique coordination mode, as bridge ligand between T and Ni atoms of neighboring layers. The incorporation of the pyrazine bridges between both metal centers leads to formation of rippled layers configuration, suggesting that the pyrazine molecule bonding interaction is stronger with the metal linked at the N end of the CN group. The resulting framework is relatively compact with a pore size below 4 Å. The H_2 adsorption in that framework shows pronounced kinetic effects and a low cavity filling related to a low H_2 diffusion rate in the system of narrow and irregular channel system. All these structural features were corroborated from IR and Raman spectra, and TG data. These solids remain stable on heating up to 130 °C and its decomposition proceeds by the lost of a pyrazine molecule to form the mono-pyrazine complex salt, which has a crystalline structure, and then about 160 °C the evolution of the second pyrazine molecule is detected.

Supplementary information

Structural information derived from the crystal structures refinement has also been deposited at ICSD Fachinformationszentrum Karlsruhe (FIZ) (E-mail: crysdatafiz-karlsruhe.de) with CSD file numbers: 419941:$Mn[Ni(CN)_4] \cdot 2pyz$; 419943:$Zn[Ni(CN)_4] \cdot 2pyz$; 419942:$Cd[Ni(CN)_4] \cdot 2pyz$. Additional supplementary information is available free of charge via the Internet at doi:10.1016/j.jssc.2008.12.028.

Acknowledgments

Appendix A. Supplementary material

Supplementary data associated with this article can be found in the online version at doi:10.1016/j.jssc.2008.12.028.

References

[1] S.M. Auerbach, K.A. Carrado, P.K. Dutta, Handbook of Layered Materials, Routledge Publishing, Taylor & Francis Group, USA, 2004.
[2] F. Bergaya, B.K. Theng, G. Lagaly, Handbook of Clay Science, Elsevier, 2006.
[3] D.S. Kim, P.M. Forster, G. Díaz de Delgado, S.-E. Park, A.K. Cheetham, Dalton Trans. (2004) 3365.
[4] R. Ishii, Y. Shinohara, J. Mater. Chem. 15 (2005) 551.
[5] S.M. Thomas, M.L. Occelli, Clays Clay Miner. 48 (2000) 304.
[6] T. Kitazawa, Y. Gomi, M. Takahashi, M. Takeda, M. Enomoto, A. Miyazaki, T. Enoki, J. Mater. Chem. 6 (1996) 119.
[7] V. Niel, J.M. Martínez-Agudo, M.C. Muñoz, A.B. Gaspar, J.A. Real, Inorg. Chem. 40 (2001) 3838.
[8] Y. Li, Y. Liu, Y. Wang, Y. Leng, L. Xie, X. Li, Int. J. Hydrogen Energy 32 (2007) 3411.
[9] J.T. Culp, S. Natesakhawat, M.R. Smith, E. Bittner, C. Matranga, B. Bockrath, J. Phys. Chem. C 112 (2008) 7079.
[10] G. Molnár, V. Niel, A.B. Gaspar, J.-A. Real, A. Zwick, A. Bousseksou, J.J. McGarvey, J. Phys. Chem. B 106 (2002) 9701.
[11] G. Molnár, V. Niel, J.-A. Real, L. Dubrovisnky, A. Bousseksou, J.J. McGarvey, J. Phys. Chem. B 107 (2003) 3149.
[12] T. Tayagaki, A. Galet, G. Molnár, M.C. Muñoz, K. Tanaka, J.-A. Real, A. Bousseksou, J. Phys. Chem. B 109 (2005) 14859.
[13] S.-I. Nishikiori, H. Yoshikawa, Y. Sano, T. Iwamoto, Acc. Chem. Res. 38 (2005) 227 and references therein.
[14] G.M. Sheldrick, Program for Crystal Structure Determination, Institute fur Anorg. Chemie, Göttingen, Germany, 1997.
[15] A.L. Le Bail, ESPOIR: A program for solving structures by Monte Carlo from powder diffraction data, in EPDIC-7, Barcelona, 2000 ⟨http://www.cristal.org/sdpd/espoir/S⟩.
[16] J. Rodríguez-Carvajal, FullProf 2005 Program, Institute Louis Brillouin, Saclay, France, 2005.
[17] T. Hasegawa, T. Iwamoto, J. Incl. Phenom. 6 (1988) 549.
[18] E. Reguera, E. Marín, A. Calderón, J. Rodríguez-Hernández, Spectrochim. Acta A 68 (2007) 191.
[19] T. Akyuz, S. Akyuz, J.E.D. Davies, J. Incl. Phenom. Mol. Recogn. Chem. 9 (1990) 349.
[20] T. Otieno, S.J. Retting, R.C. Thompson, J. Trotter, Can. J. Chem. 67 (1989) 1964.
[21] J. Balmaseda, E. Reguera, J. Rodríguez-Hernández, L. Reguera, M. Autie, Micropor. Mesopor. Mater. 96 (2006) 222.
[22] J. Roque, E. Reguera, J. Balmaseda, J. Rodríguez-Hernández, L. Reguera, L.F. del Castillo, Micropor. Mesopor. Mater. 103 (2007) 57.
[23] R.V.R.A. Ríos, J. Silvestre-Albero, A. Sepúlveda-Escribano, M. Molina-Sabio, F. Rodríguez-Reinoso, J. Phys. Chem. C 111 (2007) 3803.